# Site Sensitivity of Interfacial Charge Transfer and Photocatalytic Efficiency in Photocatalysis

Cong Fu,[+] Fei Li,[+] Jiachen Zhang,[+] Dan Li, Kun Qian, Yong Liu, Junwang Tang, Fengtao Fan, Qun Zhang,* Xue-Qing Gong,* Weixin Huang*

Abstract: Understanding structural effects and reaction mechanisms of photocatalysts is of great interest and importance. Herein we report a comprehensive study of photocatalytic oxidation of methanol on various anatase TiO_2 nanocrystals by means of combined in situ and time-resolved characterizations and density functional theory calculations. Surface site and resulting surface adsorbates were observed to strongly affect the surface band bending/bulk-to-surface charge migration processes and the interfacial electronic structure/interfacial charge transfer processes. TiO_2 nanocrystals predominantly enclosed by the {001} facets expose a high density of reactive fourfold-coordinated Ti sites (Ti_{4c}) at which CH_3OH molecules dissociate to form the CH_3O adsorbate ($CH_3O(a)_{Ti4c}$). $CH_3O(a)_{Ti4c}$ exhibits the localized density of states almost at the valence band maximum of TiO_2 surface, which facilitates the interfacial hole transfer process; meanwhile, $CH_3O(a)_{Ti4c}$ with a high coverage greatly promotes the upward surface band bending, which facilitates the bulk-to-surface hole migration process. Consequently, among all the observed surface adsorbates, $CH_3O(a)_{Ti4c}$ exhibits the highest photocatalytic oxidation rate constant. Consequently, TiO_2 nanocrystals predominantly enclosed by the {001} facets are most active in photocatalytic methanol oxidation reaction. These results unambiguously exemplify the surface structure effect in photocatalysis and elucidate the underlying mechanism.

[*]   C. Fu,[+] D. Li, K. Qian, Prof. W. Huang
        Hefei National Laboratory for Physical Sciences at the Microscale,
        Key Laboratory of Surface and Interface Chemistry and Energy
        Catalysis of Anhui Higher Education Institutes, CAS Key Laboratory
        of Materials for Energy Conversion and Department of Chemical
        Physics, University of Science and Technology of China
        Heifei 230026 (P. R. China)
        E-mail: huangwx@ustc.edu.cn
        F. Li,[+] Prof. X. Gong
        Key Laboratory for Advanced Materials, Centre for Computational
        Chemistry and Research Institute of Industrial Catalysis, East China
        University of Science and Technology,
        Shanghai 200237 (P. R. China)
        E-mail: xgong@ecust.edu.cn
        J. Zhang,[+] Prof. Q. Zhang
        Hefei National Laboratory for Physical Sciences at the Microscale,
        Department of Chemical Physics, Synergetic Innovation Center of
        Quantum Information and Quantum Physics, University of Science
        and Technology of China
        Heifei 230026 (P. R. China)
        E-mail: qunzh@ustc.edu.cn
        Y. Liu, Prof. F. Fan
        State Key Laboratory of Catalysis, Dalian Institute of Chemical
        Physics, Chinese Academy of Sciences
        Dalian 116023 (P. R. China)
        Prof. J. Tang
        Department of Chemical Engineering, University College London
        London, WC1E 7JE (UK)
        Prof. F. Fan, Prof. W. Huang
        Dalian National Laboratory for Clean Energy
        Dalian 116023 (P. R. China)
[†]   These authors contributed equally to this work.

        Supporting information for this article is given via a link at the end of
        the document.

Introduction

Since the pioneering work on photocatalysis by Honda and Fujishima in 1972,[1] semiconductor-based photocatalysis has attracted extensive attention due to the utilization of sustainable solar energy for chemical fuel production, environmental remedy and chemical synthesis.[2] A photocatalytic reaction consists of light absorption and charge generation within photocatalysts, charge separation and migration to photocatalyst surfaces, and charge-participated reactions on photocatalyst surfaces (Scheme 1A). The first two steps mainly occur in the bulk of photocatalysts, and significant progresses have been achieved in maximizing their efficiencies via structural optimizations.[3] The last step involves an interfacial charge transfer process from photocatalyst surfaces to surface adsorbates and subsequent surface reactions. Thus it is the rate-limiting step of photocatalytic reactions, however, it has been much less studied due to the complexity.
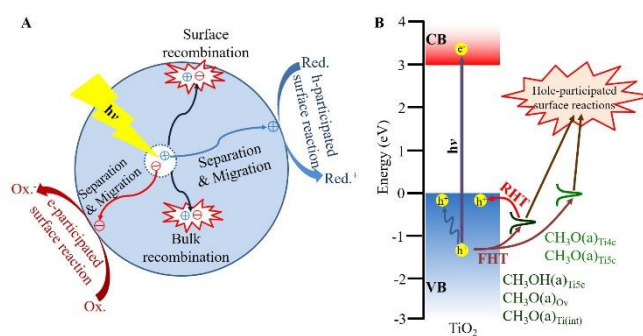
Scheme 1. Schematic Illustration of (A) fundamental processes of surface photocatalysis and (B) adsorbate-dependent methanol/TiO_2 interfacial hole transfer processes. "FHT" and "RHT" mean the TiO_2-to-methanol forward hole transfer and methanol-to-TiO_2 reverse hole transfer, respectively.

Photocatalytic conversions of CH_3OH on TiO_2 are prominent in environmental photocatalytic reactions, photocatalytic selective oxidation and photocatalytic reforming reactions, and are used as a hole scavenging reaction to enhance the efficiency of photocatalytic water splitting to hydrogen.[4] Meanwhile, they are extensively adopted as the probe photocatalytic reaction for fundamental studies of complex photocatalytic reactions on oxide photocatalysts. Therefore, adsorption and photochemistry of CH_3OH has been much explored using well-defined TiO_2 single crystals and nanocrystals (NCs) as model photocatalysts.[5] CH_3OH mainly adsorbs molecularly at the fivefold-coordinated Ti_{5c} sites on the TiO_2 surfaces ($CH_3OH(a)_{Ti5c}$), and dissociates at the surface oxygen vacancy sites, subsurface interstitial Ti^{3+}-related sites and fourfold-coordinated Ti_{4c} sites to form the methoxy species ($CH_3O(a)$).[6] On rutile $TiO_2(110)$ surface, it is argued whether the $CH_3OH(a)_{Ti5c}$ dissociation to the $CH_3O(a)$ species at the Ti_{5c} site ($CH_3O(a)_{Ti5c}$) on TiO_2 surfaces is induced only thermally [7] or can be photocatalytically.[8] The $CH_3O(a)_{Ti5c}$

species is photocatalytic active to undergo the C-H bond breaking to form the HCHO(a) species;[7-9] moreover, the photo-induced oxidative coupling reaction between co-adsorbed $CH_3O(a)$ and HCHO(a) at the Ti_{5c} sites were observed to produce methyl formate ($HCOOCH_3$).[10] The $CH_3O(a)_{Ti5C}$ is more photoreactive on rutile $TiO_2(110)$ surface than on rutile $TiO_2(011)$-(2×1) surface.[10d,10e] On anatase $TiO_2(001)$-(1×4) surface, photocatalytic oxidation was observed to occur specifically for the $CH_3O(a)$ species at the Ti_{4c} site ($CH_3O(a)_{Ti4c}$) without the further formation of $HCOOCH_3$.[11] Photo-oxidation of methanol on nanocrystalline anatase TiO_2 showed that bipyramidal nanoparticles exposing primarily {101} facets were more active than platelets exposing primarily {001} surfaces, whereas the platelets were more active for thermally-driven reactions.[12] Efficient photocatalytic conversions of methanol molecules over TiO_2 nanoparticles were found to require the presence of O_2,[13,14] which acts to promote methanol photodecomposition to form $CH_3O(a)$, scavenge free electrons and open acceptor sites for the injection of new electrons during $CH_3O(a)$ oxidation, and interact with surface intermediates.

The TiO_2-to-methanol interfacial hole transfer process at the CH_3OH/TiO_2 interfaces plays a key role in photocatalytic methanol oxidation. The hole transfer dynamics from photoexcited nanocrystalline TiO_2 film to adsorbed alcohols was measured by highly sensitive femtosecond and nanosecond spectroscopy under low intensity excitation conditions to avoid fast electron-hole recombination, from which the rates and yields of photocatalytic oxidation of the studied alcohols on TiO_2 were evaluated.[15] By measuring the kinetic competition of holes between recombination with electrons and reaction with methanol, it was concluded that the lower photocatalytic activity of rutile TiO_2 than anatase TiO_2 was not due to differences in recombination but rather to the deficiency of holes to drive efficient and irreversible alcohol oxidation, likely related to surface structure and reactive surface species.[16] Theoretical calculation results of photoexcited hole dynamics at the CH_3OH/rutile $TiO_2(110)$ interface suggested that only the $CH_3O(a)_{Ti5c}$ species can scavenge the photoexcited holes due to its favorable energy level alignment at the interface.[17]

Thus, the interfacial hole transfer and photochemistry of CH_3OH on TiO_2 depend on the TiO_2 surface structure and the adsorbed methanol species, but the underlying mechanism and the correlation with the photocatalytic efficiency have not been established. Herein, we comprehensively studied photochemistry of CH_3OH oxidation on various TiO_2 NCs and influences of water coadsorption by means of *in situ* and time-resolved diffuse-reflectance infrared spectroscopy (DRIFTS), *in situ* electron paramagnetic resonance spectroscopy (ESR), *in situ* surface photovoltage (SPV) measurements, time-resolved photoluminescence spectroscopy (PL) and *in situ* femtosecond time-resolved transient absorption (*fs*-TA) spectroscopy, in combination with density functional theory (DFT) calculations. The surface site and corresponding adsorbed methanol species are successfully demonstrated to determine the TiO_2-to-CH_3OH interfacial charge transfer process and subsequently the photocatalytic efficiency, providing compelling evidence for the surface structural effect of photocatalysts on the photocatalysis.

Results and Discussion

Three types of anatase TiO_2 NCs primarily enclosed with {001}, {100} and {101} facets, respectively denoted as TiO_2-{001}, TiO_2-{100} and TiO_2-{101}, were synthesized following previous recipes[18] and characterized microscopically and spectroscopically (Fig. 1 a-c, Supplementary Figs. 1-3). All samples exhibit a pure anatase phase, uniform morphologies, similar average sizes of around 12 nm, and similar specific surface areas of ~100 m^2/g. The percentages of {001} facets in TiO_2-{001}, {100} facets in TiO_2-{100}, and {101} facets in TiO_2-{101} NCs were estimated to be around 80%.[18] Commonly observed adsorbates resulting from ambient CO_2 and H_2O adsorption, such as carbonates, hydroxyl and water, are present on the surfaces of TiO_2 NCs, but the capping ligands (F^-, SO_4^{2-} and Cl^-) used during the synthesis were not detected.
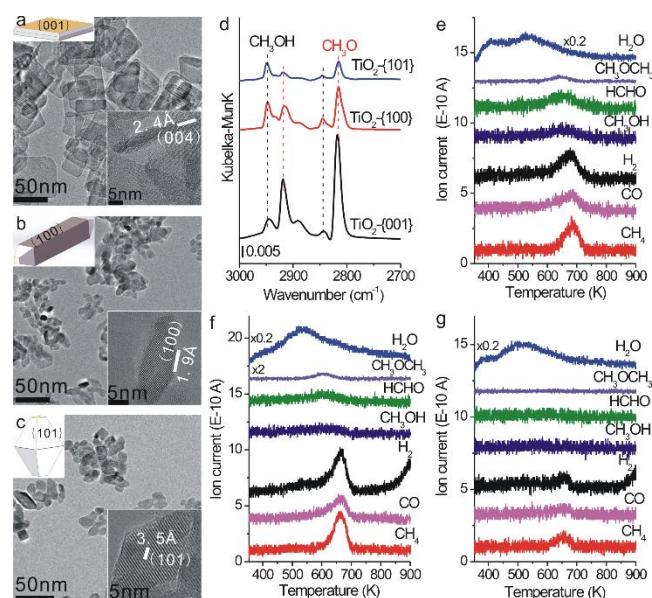

Figure 1. Representative TEM images with inserted HRTEM images and schematic morphology illustrations of (a) TiO_2-{001}, (b) TiO_2-{100} and (c) TiO_2-{101} NCs. (d) DRIFTS spectra following CH_3OH adsorption on various TiO_2 NCs at 313 K, with DRIFTS spectra of corresponding bare TiO_2 NCs as the background spectra. TPD spectra following CH_3OH adsorption at 353 K with a heating rate of 10 K/min on (e) TiO_2-{001}, (f) TiO_2-{100} and (g) TiO_2-{101} NCs.

Adsorption and surface reaction of CH_3OH were used to probe the surface structures of as-synthesized TiO_2 NCs. As shown in Figure 1d, CH_3OH adsorption at 313 K gives rise to the vibrational bands of $CH_3OH(a)$ and $CH_3O(a)$ at 2850/2950 and 2820/2920 cm^{-1}, respectively.[19] The vibrational peak of $CH_3OH(a)$ on TiO_2-{100} is stronger than on TiO_2-{001} and TiO_2-{101}, while the vibrational peak intensities of $CH_3O(a)$ differ greatly and follow an order of TiO_2-{001} >> TiO_2-{100} > TiO_2-{101}. Thus, TiO_2-{001} exhibits the largest $CH_3O(a)$:$CH_3OH(a)$ ratio among the studied TiO_2 nanocrystals while TiO_2-{101} exhibits the smallest. The vibrational bands of OH groups on TiO_2 NCs were found to reduce greatly upon CH_3OH adsorption (Supplementary Fig. 4), demonstrating that CH_3OH adsorption can displace the OH groups originally on TiO_2 NCs, consistent with previous reports.[20] Since the formation of $CH_3O(a)$ species upon CH_3OH dissociation is accompanied by the OH formation, the loss of OH vibrational bands follows an order of TiO_2-{001} < TiO_2-{100} < TiO_2-{101}, inverse to that of $CH_3O(a)$ formation.

TiO$_2$ NCs exclusively with CH$_3$O(a) species were prepared by CH$_3$OH adsorption at 353 K and the reactivity of CH$_3$O(a) was studied with TPD spectra (Fig. 1 e–g). A water desorption peak at 550 K appears for all TiO$_2$ NCs and can be attributed to the recombinative desorption of OH groups. An additional water desorption peak at 425 K arises only for TiO$_2$-{001} and can be attributed to the desorption of H$_2$O(a) at the Ti sites. With the temperature increasing, the CH$_3$O(a) species undergoes bi-molecular dehydration coupling reaction to produce CH$_3$OCH$_3$, bi-molecular disproportionation reaction to simultaneously produce CH$_3$OH and HCHO, unimolecular dehydrogenation reaction to produce CO and H$_2$, and unimolecular deoxy-hydrogenation reaction to produce CH$_4$. The amounts of total detected products from CH$_3$O(a)/TiO$_2$ NCs decrease from CH$_3$O(a)/TiO$_2$-{001} to CH$_3$O(a)/TiO$_2$-{100} and further to CH$_3$O(a)/TiO$_2$-{101}, consistent with the order of the CH$_3$O(a) coverage on TiO$_2$ NCs. Meanwhile, the bi-molecular reaction probability of CH$_3$O(a) species also decreases with the coverage of CH$_3$O(a) species on TiO$_2$ NCs. The CH$_3$O(a) species on TiO$_2$-{100} undergo all bi-molecular and unimolecular reactions, but the probability of bi-molecular reactions is much smaller than that on TiO$_2$-{001}. The CH$_3$O(a) species on TiO$_2$-{101} only undergo the unimolecular reactions but not the bi-molecular reactions. Similar results were previously reported on surface reactions of methanol on the TiO$_2$-{001} and TiO$_2$-{101} nanocrystals.[12b,21]

Adsorption and surface reaction of CH$_3$OH on various TiO$_2$ single crystal surfaces have been well established.[5] The observed reactivity of CH$_3$O(a) species at TiO$_2$-{001} are very similar to those on the restructured anatase TiO$_2$(001)-(1×4) single crystal surface exposing the reactive Ti$_{4c}$ sites at the (1×4) added row and the Ti$_{5c}$ sites at the (1×1) basal surface (Supplementary Fig. 5).[6c] The (1×4) surface restructuring of {001} facets at TiO$_2$-{001} was previously confirmed by ^{17}O solid-state NMR spectroscopy[22] and environmental transmission electron microscopy.[23] The observed reactivity of CH$_3$O(a) species on TiO$_2$-{101} are similar to those on the anatase TiO$_2$(101) single crystal surface with minor surface oxygen vacancies (Supplementary Fig. 6).[24] No studies of CH$_3$OH on the anatase TiO$_2$(100) single crystal surface was reported, but STM and XPS characterization results show that the anatase TiO$_2$(100) single crystal surface exhibits a typical (1×2) restructured surface with the presence of interstitial Ti^{3+} defects and the absence of surface oxygen vacancy defects (Supplementary Fig. 7).[25] DFT calculations were performed for CH$_3$OH adsorption on the anatase TiO$_2$(001)-(1×4) surface, TiO$_2$(101) surfaces with and without surface oxygen vacancies, and TiO$_2$(100)-(1×2) with and without subsurface interstitial Ti^{3+} defects. CH$_3$OH adsorbs dissociatively at the Ti$_{4c}$ site of anatase TiO$_2$(001)-(1×4) (CH$_3$O(a)$_{Ti4c}$) with an adsorption energy of 2.82 eV and molecularly at the Ti$_{5c}$ site (CH$_3$OH(a)$_{Ti5c}$) with an adsorption energy of 0.66 eV (Figure 2 and Supplementary Fig. 5). The molecular adsorption energy (1.27 eV) of CH$_3$OH(a)$_{Ti5c}$ at the Ti$_{5c}$ site of perfect TiO$_2$(101) is larger than the dissociative adsorption energy (1.10 eV) of CH$_3$OH (CH$_3$O(a)$_{Ti5c}$), suggesting a preferential molecular adsorption at the Ti$_{5c}$ sites, while CH$_3$OH preferentially dissociates at the minor surface oxygen vacancy site (CH$_3$O(a)$_{Ov}$) and molecularly adsorbs at the minor Ti$_{5c}$ site next to the surface oxygen vacancy sites (CH$_3$OH(a)$_{Ti5c(Ov)}$), respectively with adsorption energies of 2.48 and 1.05 eV (Figure 2 and Supplementary Fig. 6). The adsorption energies of CH$_3$O(a)$_{Ti5c}$ and CH$_3$OH(a)$_{Ti5c}$ at the Ti$_{5c}$ site of perfect TiO$_2$(100)-

(1×2) are almost identical, respectively being 1.30 and 1.26 eV, while the dissociative (CH$_3$O(a)$_{Ti(int)}$) and molecular (CH$_3$OH(a)$_{Ti(int)}$) adsorption of CH$_3$OH at the minor Ti$_{5c}$ site neighbouring to the subsurface interstitial Ti^{3+} site give adsorption energies respectively of 1.64 and 1.33 eV (Figure 2 and Supplementary Fig. 7), suggesting a preferential dissociation. Similar subsurface interstitial Ti^{3+} site-induced dissociation of CH$_3$OH was previously reported on the rutile TiO$_2$(110) single crystal surface.[6b] Considering the densities of the sites on various TiO$_2$ favoring the CH$_3$OH dissociative adsorption and the associated differences between molecular and dissociative adsorption energies, the DFT calculation results suggest that the density of CH$_3$O(a) species is largest on TiO$_2$(001)-(1×4) surface and least on TiO$_2$(101) surface, consistent with the above DRIFTS results. They also indicate that the CH$_3$O(a)$_{Ti5c}$ species is more on TiO$_2$-{100} than on TiO$_2$-{101} but is few on TiO$_2$-{001}.
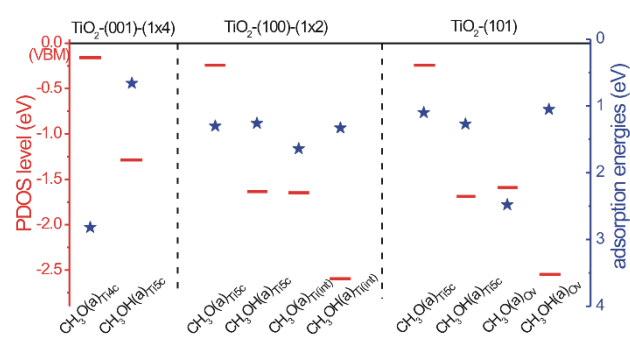

Figure 2. Calculated adsorption energies and PDOS levels relative to the valence band maximum of various types of methanol adsorbates on anatase TiO$_2$ surfaces.

The evolutions of CH$_3$OH(a) and CH$_3$O(a) at various TiO$_2$ NCs upon UV light illumination were studied using *in situ* DRIFTS spectra. In the absence of O$_2$, a large increase in the absorbance across the entire spectrum arising from the absorption of photoexcited electrons[26] was observed for bare TiO$_2$-{001} but not for bare TiO$_2$-{100} and TiO$_2$-{101} (Supplementary Fig. 8), indicating much more abundant photoexcited electrons created in TiO$_2$-{001} than in TiO$_2$-{100} and TiO$_2$-{101}. Upon CH$_3$OH adsorption, the density of photoexcited electrons greatly increased for all TiO$_2$ NCs, due to the efficient trapping of photoexcited holes by the adsorbed methanol species and the subsequent enhanced accumulation of photoexcited electrons. However, no obvious conversions of adsorbed CH$_3$O(a) and CH$_3$OH(a) species could be observed (Supplementary Fig. 9), consistent with previous results [13] that the accumulated photoexcited electrons could block acceptor sites on TiO$_2$ surface for the injection of new electrons required by the photocatalytic oxidation of adsorbed methanol species.

With the introduction of O$_2$, O$_2$-promoted CH$_3$OH(a) dissociation to CH$_3$O(a) [27] was observed to occur only slightly for all TiO$_2$ NCs under the dark condition (Supplementary Fig. 10). Upon UV light illumination, the absorption feature of photoexcited electrons greatly decreased with the O$_2$ concentration increasing, and became similar for all TiO$_2$ NCs at an oxygen concentration of 10% (Supplementary Fig. 11), demonstrating the efficient scavenging of photoexcited electrons by O$_2$. Consequently, photocatalytic oxidation of adsorbed CH$_3$O(a) species to HCOO(a), HCHO(a) and carbonate species occur on all TiO$_2$ NCs,

as evidenced by the appearance of the vibrational features of various types of HCOO(a) and carbonate species and HCHO(a) species [13,28] at the expense of those of $CH_3O(a)$ species (Supplementary Fig. 12, Supplementary Table 1). The further photocatalytic oxidation of HCOO(a) species forms gaseous CO_2, the final product of photocatalytic CH_3OH oxidation in O_2. Although the photocatalytic oxidation of methanol produces H^+ species in the form of OH groups TiO_2 surfaces, the OH groups on during the photocatalytic oxidation of methanol adsorbates change little. This suggests that the generated H^+ species should facilely undergo photoexcited electrons-participated reduction reactions with adsorbed O_2 to produce gaseous water. The amounts of adsorbed O_2 on various TiO_2 NCs were measured to be similar (Supplementary Fig. 13).
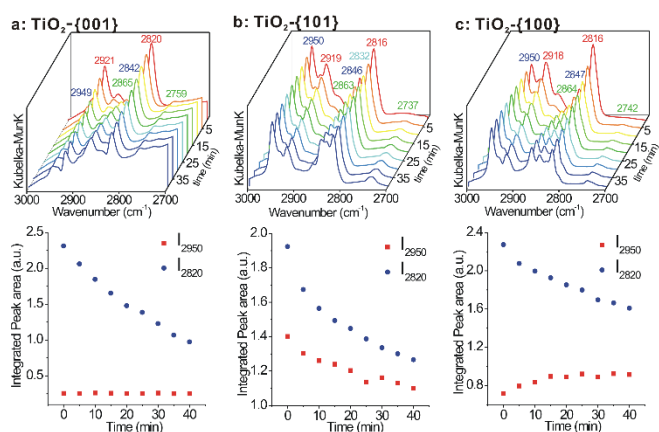
Figure 3. (Top) In-situ and time-resolved DRIFTS spectra of photocatalytic oxidation of $CH_3O(a)$ and $CH_3OH(a)$ at 313 K in a 10% O_2/Ar atmosphere with a flow rate of 30 cm^3/min and (Bottom) coverages of $CH_3O(a)$ and $CH_3OH(a)$, respectively represented by the integrated intensity of the vibrational features at 2820 and 2950 cm^{-1}, as a function of photocatalytic oxidation time: (a) TiO_2-{001}, (b) TiO_2-{101} and (c) TiO_2-{100} NCs. DRIFTS spectra of corresponding bare TiO_2 NCs were used as the background spectra.

The photocatalytic oxidation kinetics of $CH_3OH(a)$ and $CH_3O(a)$ species on various TiO_2 NCs in a 10% O_2/Ar atmosphere were further studied using in-situ and time-resolved DRIFTS spectroscopy. Under this condition the photoexcited charge carrier density in TiO_2 NCs and the photoexcited electrons-participated surface reactions of H^+ and O_2 are similar for various TiO_2 NCs. The acquired spectra were peak-fitted (Supplementary Figs. 14-16), and the derived integrated peak areas of the features at 2950 and 2820 cm^{-1}, respectively representing the surface coverages of $CH_3OH(a)$ and $CH_3O(a)$, were plotted as a function of photocatalytic oxidation time. With the UV light illumination prolonging, the vibrational features of $CH_3OH(a)$ species barely change on TiO_2-{001} (Fig. 2a), the vibrational features of $CH_3O(a)$ species keep decreasing, and the vibrational features of HCOO(a) species emerge and grow; the vibrational features of both $CH_3OH(a)$ and $CH_3O(a)$ species decrease on TiO_2-{101} (Fig. 2b), and the vibrational features of HCHO(a) species and HCOO(a) species appear and grow; the vibrational features of $CH_3OH(a)$ species increase on TiO_2-{100} NCs (Fig. 2c), the vibrational features of $CH_3O(a)$ species decrease, and those of HCOO(a) species emerge and grow.

Therefore, the $CH_3OH(a)_{Ti5c}$ species is photoinactive on TiO_2-{001} while the $CH_3O(a)_{Ti4c}$ species is photoactive, consistent with previous results on the anatase $TiO_2(001)$-(1×4) surface that UV

light illumination leads to photocatalytic oxidation of the $CH_3O(a)_{Ti4c}$ species but not of the $CH_3OH(a)_{Ti5c}$ species.[11] Both $CH_3O(a)$ and $CH_3OH(a)$ species are photoactive on TiO_2-{101}, agreeing with previous results on the anatase TiO_2 (101) surface that UV light illumination leads to photocatalytic oxidation of both $CH_3OH(a)$ and $CH_3O(a)$ species.[9b] The $CH_3O(a)_{Ti5c}$ species is photoactive on TiO_2-{100}, and the formation of $CH_3OH(a)$ upon UV light illumination can be attributed to a thermal transformation of $CH_3O(a)$ species to $CH_3OH(a)$ species induced by an oxidation of the subsurface interstitial Ti^{3+} sites of TiO_2-{100} NCs by photoexcited holes. Similar processes were proposed for photo stimulated desorption of $O_2(a)$ species related to the subsurface interstitial Ti^{3+} sites of rutile $TiO_2(110)$ single crystal surface.[29] Meanwhile, the HCOO(a) species appears as the dominant surface intermediate during photocatalytic CH_3OH oxidation on TiO_2-{001} and TiO_2-{100} while both HCHO(a) and HCOO(a) species appear on TiO_2-{101}, indicating more facile photocatalytic oxidation of HCHO(a) species on TiO_2-{001} and TiO_2-{100} than on TiO_2-{101}.
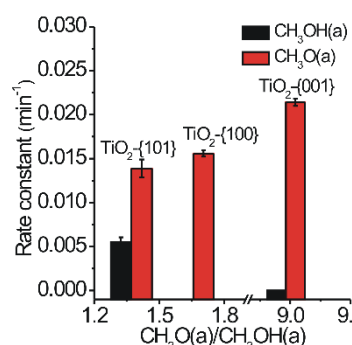

Figure 4. Rate constants of $CH_3O(a)$ and $CH_3OH(a)$ photocatalytic oxidation on various TiO_2 NCs at 313 K in a 10% O_2/Ar atmosphere with a flow rate of 30 cm^3/min as a function of initial $CH_3O(a)/CH_3OH(a)$ coverage ratios.

On TiO_2-{001}, the $CH_3OH(a)$ coverage does not change with the photocatalytic reaction time, thus the variation of $CH_3O(a)$ coverage results only from the photocatalytic oxidation reaction. The Ln (I_{2820}) was found to decrease linearly as a function of photocatalytic reaction time (Supplementary Fig. 17), demonstrating that photocatalytic oxidation of $CH_3O(a)$ on TiO_2-{001} follows the first-order reaction kinetics with a rate constant of 0.0214±0.0004 min^{-1}. The photocatalytic oxidation kinetics of $CH_3O(a)$ on TiO_2-{100} and $CH_3O(a)$ and $CH_3OH(a)$ on TiO_2-{101} were analyzed similarly (Supplementary Figs. 18 and 19), found to follow first-order reaction kinetics, yielding a rate constant of photocatalytic $CH_3O(a)$ oxidation on TiO_2-{100} as 0.156±0.0004 min^{-1} and rate constants of photocatalytic $CH_3O(a)$ and $CH_3OH(a)$ oxidation on TiO_2-{101} respectively as 0.0139±0.0002 and 0.0055±0.0006 min^{-1}. Thus, the rate constants of photocatalytic $CH_3O(a)$ oxidation follow an order of $CH_3O(a)/TiO_2$-{001} > $CH_3O(a)/TiO_2$-{100} > $CH_3O(a)/TiO_2$-{101}, which, as shown in Fig. 4, was found to correlate well with the $CH_3O(a):CH_3OH(a)$ ratio on various TiO_2 NCs. This suggests that the TiO_2 NCs with larger $CH_3O(a)$ coverage and $CH_3O(a):CH_3OH(a)$ ratio exhibit a higher rate constant of photocatalytic $CH_3O(a)$ oxidation. Meanwhile, the rate constant of photocatalytic $CH_3O(a)$ oxidation on TiO_2-{101} with dominant and photoactive $CH_3OH(a)$ species is still larger than that of photocatalytic $CH_3OH(a)$ oxidation, which,

agreeing with the case of TiO₂-{001}, confirms that the CH₃O(a) species on TiO₂ is intrinsically more photoactive than the CH₃OH(a) species.

The observed first-order photocatalytic oxidation kinetics of CH₃O(a) and CH₃OH(a) suggests that the photoexcited hole concentrations at the methanol/TiO₂ interfaces are large enough to be considered as constants. Therefore, the photocatalytic oxidation rate constant strongly depends on the photoexcited hole concentration at the methanol/TiO₂ interface and the TiO₂-to-methanol interfacial hole transfer efficiency. Various TiO₂ NCs were measured to exhibit almost identical UV-Vis diffuse reflectance spectra and similar valence band photoelectron spectra (Supplementary Fig. 20), and thus they should exhibit similar processes of light absorption and charge generation. The kinetics of photogenerated charges were then characterized with femtosecond time-resolved transient absorption (*fs*-TA) spectroscopy using a pump−probe configuration of a 320 nm pump and a white-light (360–700 nm) probe (Supplementary Fig. 21). The TA signals of photo-excited electrons in TiO₂ were identified in the near-infrared and infrared spectral regions, while those of photoexcited holes in the UV and near-visible regions (up to 500 nm).[30] Although the TA signals of photoexcited electrons and holes in TiO₂ overlap in the visible region, the observed broad, negative profile in the range of about 360-550 nm can be mainly ascribed to photo-excited hole absorptions, while the observed broad, positive profile above 550 nm to the overlapping photo-excited electron and hole absorptions in our case. The kinetic profiles of photoexcited hole absorptions within the region of 380-410 nm were analyzed for various TiO₂ NCs (Figure 5 a-c). Using a global fitting procedure, the acquired TA kinetic spectra of all TiO₂ NCs can be fitted by three components with the characteristic time constants included in Figure 5 a-c. The first two components are related to the relaxation processes of the photoexcited holes from the valence-band maximum to two trap states, probably with different trap depths.[31] Indicated either by individual kinetic parameters of three components or by the average kinetic parameter, TiO₂-{001} NCs exhibit much faster relaxation processes of photoexcited holes than other two TiO₂ NCs, which suggest the presence of more hole trap states in TiO₂-{001} NCs.

TiO₂ NCs upon UV light illumination were characterized with ESR spectroscopy (Supplementary Fig. 22). TiO₂-{001} mainly exhibit the signals of F^{1+} color centers and adsorbed O_2^- species, while TiO₂-{100} and TiO₂-{101} mainly exhibit the signals of F^{1+} color centers, consistent with previous reports.[32] Upon UV light illumination, the photoexcited electrons trapped in the bulk and on the surface of TiO₂ NCs give rise to the Ti^{3+} signal and enhance the ability of TiO₂ to chemisorb O_2 in the ambient condition to form the O_2^- species, respectively; meanwhile, the trapped holes generate the O^- species.[33] The resulting Ti^{3+}, O_2^- and O^- signals are much stronger for TiO₂-{001} NCs than for TiO₂-{100} and TiO₂-{101} NCs, which, consistent with the above TA results, demonstrates more effective trapping of photoexcited electrons and holes in TiO₂-{001} NCs.

The recombination processes of photoexcited electrons and holes were studied with both steady-state and time-resolved photoluminescence (PL) spectra. The steady-state PL spectra (Supplementary Fig. 23) show that all TiO₂ NCs exhibit a major peak at ~520 nm with two shoulders at ~423 and ~635 nm, attributed to the radiative recombination at oxygen vacancies, lattice imperfections and Ti^{3+} sites.[32] TiO₂-{001} NCs show a

greatly stronger PL peak at ~520 nm than other two TiO₂ NCs, thus TiO₂-{001} NCs have the largest density of oxygen vacancies that can act as the hole trap sites. The time-resolved PL spectra with an excitation at 368 nm and an emission at 515 nm (Fig. 5 d-f) demonstrate that the photoexcited electrons and holes within TiO₂-{001} NCs recombine faster than within TiO₂-{100} and TiO₂-{101} NCs.
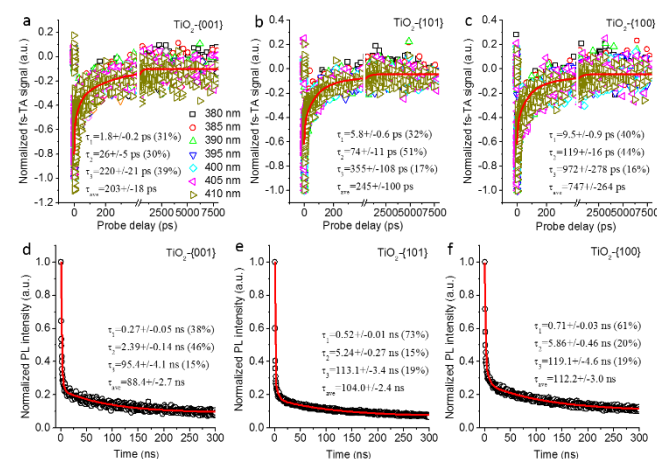
Figure 5. Representative TA kinetics of (a) TiO₂-{001}, (b) TiO₂-{101} and (c) TiO₂-{100} NCs in air taken at the pump wavelength of 320 nm and the probing wavelength from 380 to 410 nm. Time-resolved PL kinetics of (d) TiO₂-{001}, (e) TiO₂-{101} and (f) TiO₂-{100} NCs in air recorded with excitation at 368 nm and emission at 515 nm.

Thus, TiO₂-{001} NCs with the largest density of oxygen vacancies as the hole trap sites exhibit the fastest relaxation processes of photoexcited holes and meanwhile the fastest recombination process of photoexcited electrons and holes. These observations suggest that the defects in TiO₂ facilitate not only the charge separation processes but also the charge recombination processes. Different bulk charge carrier dynamics in anatase and rutile TiO₂ single crystals were observed to demonstrate bulk defects-resulted fast recombination rates through trap-state-assisted channel of charge recombination and to explain the substantially higher activity of anatase TiO₂ in photocatalytic CO oxidation.[34] A recent pulsed-laser-combined scanning tunneling microscopy and spectroscopy study of rutile TiO₂(110) surface also proposed that the lifetime of photoexcited free electrons was correlated with the averaged defect density within a nanometer-sized area.[35]

The separated photoexcited charges need to migrate from the bulk of a photocatalyst particle to the surface to participate the surface redox reactions, which is strongly affected by the surface band bending of the photocatalyst.[36] We measured surface photovoltage (SPV) signals of TiO₂ NCs and methanol/TiO₂ NCs generated upon UV light illumination (Fig. 6 and Supplementary Fig. 24). TiO₂ NCs exhibit the positive SPV signals arising from an upward surface band bending that facilitates the hole migration from the bulk to the surface. The SPV signals of TiO₂-{001} and TiO₂-{100} are similar and larger than that of TiO₂-{101}, which can be attributed to the (1×4) surface reconstruction of TiO₂-{001} and the presence of subsurface interstitial Ti^{3+} sites in TiO₂-{100}. CH₃OH adsorption greatly enhances the SPV signals of both TiO₂-{001} and TiO₂-{101} NCs but reduces that of TiO₂-{100} NCs. CH₃OH(a) at TiO₂ surfaces can act as an electron donor,

5

weakening the upward surface band bending, whereas $CH_3O(a)$ at TiO_2 surfaces can act as an electron acceptor, strengthening the upward surface band bending.[36] Thus CH_3OH/TiO_2-{001} with dominant $CH_3O(a)$ species and CH_3OH/TiO_2-{101} with more $CH_3O(a)$ than $CH_3OH(a)$ exhibit strengthened upward surface band bending, while CH_3OH/TiO_2-{100} with more $CH_3OH(a)$ than $CH_3O(a)$ exhibits weakened upward surface band bending. The decreased subsurface interstitial Ti^{3+} concentration of $CH_3OH/TiO_2(100)$ under UV light illumination (Fig. 3c) can also weaken the upward surface band bending. As indicated by the SPV signals, the upward surface band bending extent and the bulk-to-surface hole migration process follows an order of CH_3OH/TiO_2-{001} > CH_3OH/TiO_2-{101} > CH_3OH/TiO_2-{100}.
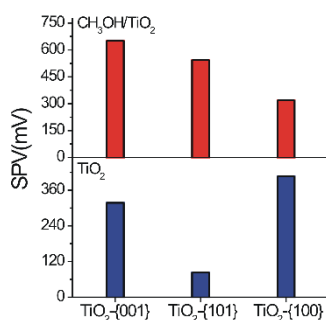

Figure 6. Surface photovoltage (SPV) amplitudes of as-synthesize and methanol-covered TiO_2 NCs generated upon UV light illumination.

The dynamics of photoexcited holes of CH_3OH/TiO_2 (TiO_2 NCs dispersed in methanol) were probed with *fs*-TA spectroscopy using a pump−probe configuration of a 320 nm pump and a 450 nm probe (Fig. 7 and Supplementary Fig. 25). Similar to the bare TiO_2 sample, CH_3OH/TiO_2-{001} exhibits a monotonic recovery of probe bleach (PB) with time (Fig. 7a), corresponding to the hole trapping and recombination processes. In addition to the hole trapping and recombination processes, both CH_3OH/TiO_2-{100} and CH_3OH/TiO_2-{101} exhibit a turn-around PB growth beyond ~30 ps, demonstrating the occurrence of additional hole transfer process. CH_3OH adsorbates on TiO_2 are known to scavenge the photoexcited holes, therefore, the observed PB growth superimposing on the relaxation trace of photoexcited holes corresponds to the photo-induced absorption of a reverse hole transfer (RHT) process from the acceptor states of CH_3OH adsorbates to the valence band maximum (VBM) of TiO_2 NCs. A similar RHT process from adsorbed $CH_3O(a)$ to the VBM of g-C_3N_4 photocatalyst was previously observed by TA spectroscopy.[37] Therefore, CH_3OH/TiO_2-{001} with dominant $CH_3O(a)_{Ti4c}$ and minor $CH_3OH(a)_{Ti5c}$ species does not exhibit the RHT process, while CH_3OH/TiO_2-{100} with $CH_3O(a)$ and $CH_3OH(a)$ at both subsurface interstitial Ti^{3+} and surface Ti_{5c} sites and CH_3OH/TiO_2-{101} with $CH_3O(a)$ at the surface oxygen vacancy sites and $CH_3O(a)$ and $CH_3OH(a)$ at surface Ti_{5c} sites exhibit. Meanwhile, the τ value of RHT process of CH_3OH/TiO_2-{101} was fitted as 327± 65 ps, larger than that of CH_3OH/TiO_2-{100} (122 ± 15 ps)，consistent with the more extensive upward surface band bending of CH_3OH/TiO_2-{101} than of CH_3OH/TiO_2-{100}. These observations unambiguous demonstrate the site sensitivity of interfacial hole transfer processes at the CH_3OH/TiO_2 interface. TA results on the microsecond to second

time scale previously showed efficient, irreversible hole scavenging by alcohols on mesoporous anatase TiO_2 but substantially less efficient and more reversible hole scavenging by alcohols on mesoporous rutile.[16] It was then proposed that the lower photocatalytic activity of rutile was not due to differences in recombination but rather to the deficiency of rutile holes to drive efficient and irreversible alcohol oxidation.
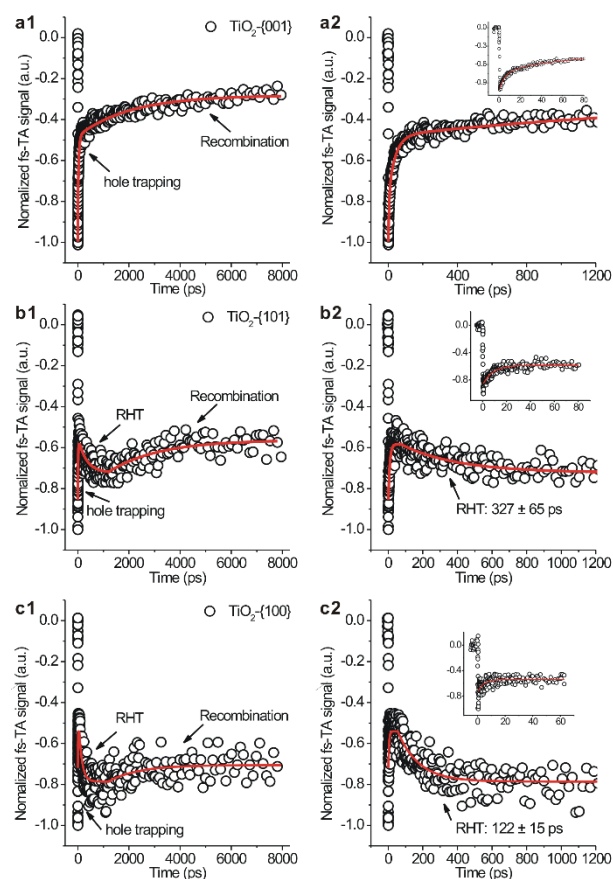

Figure 7. The PB kinetics with a pump wavelength at 320 nm and a probe wavelength at 450 nm for (a) CH_3OH /TiO_2-{001}, (b) CH_3OH/TiO_2-{101} and (c) CH_3OH/TiO_2-{100}. The inset shows expanded kinetic traces in the early-time window (0–80 ps). The RHT means reverse hole transfer from chemisorbed methanol to TiO_2.

The electronic structures of various TiO_2 and CH_3OH/TiO_2 systems were analyzed from the calculated density of states (DOS) of corresponding optimized adsorption configurations (Supplementary Figs. 5-7). The anatase $TiO_2(001)$-(1×4) surface shows the VBM and the conduction band minimum (CBM) respectively localized at the surface oxygen atoms on the added row and the bulk Ti atoms, while the $TiO_2(100)$-(1×2) surfaces without and with subsurface interstitial Ti^{3+} sites and $TiO_2(101)$ surfaces without and with surface oxygen vacancies show the VBM and CBM respectively localized at the surface oxygen atoms and the bulk Ti atoms. Upon CH_3OH adsorption, the CBM is still localized at the bulk Ti atoms, whereas the VBM involves the contributions from the CH_3OH adsorbates, depending on the adsorption structures.

As shown in Figure 2, the projected density of states (PDOS) of the $CH_3O(a)_{Ti4c}$ species on the anatase $TiO_2(001)$-(1×4) surface and the $CH_3O(a)_{Ti5c}$ species on the anatase $TiO_2(100)$-(1×2) and

6

TiO₂(101) surfaces are localized almost at the VBM of the corresponding TiO₂ surfaces, while those of CH₃OH(a)$_{Ti5c}$ species and minor CH₃OH adsorbates (CH₃O(a) and CH₃OH(a)) at the defective sites are localized far below the VBM. From the view of thermodynamics, this suggests that the CH₃O(a)$_{Ti4c}$ and CH₃O(a)$_{Ti5c}$ species have higher probabilities to accept the photogenerated holes than the CH₃OH(a)$_{Ti5c}$ species. From the view of kinetics, the transferred holes can either oxidize the CH₃OH(a)$_{Ti5c}$ species or reversely transfer to the valence band of TiO₂, whereas the transferred holes can only oxidize the CH₃O(a)$_{Ti4c}$ and CH₃O(a)$_{Ti5c}$ species. These theoretical calculation results suggest that the TiO₂-to-CH₃O(a)$_{Ti4c}$/CH₃O(a)$_{Ti5c}$ interfacial hole transfer is more efficient than the TiO₂-to-CH₃OH(a)$_{Ti5c}$ interfacial hole transfer, consistent with the observed experimental results. The CH₃O(a) species on all TiO₂ NCs are intrinsically more photoactive than the CH₃OH(a) species; meanwhile, CH₃OH/TiO₂-{100} and CH₃OH/TiO₂-{101} with high coverages of CH₃OH(a)$_{Ti5c}$ species exhibit the RHT processes, but on TiO₂-{001} with dominant CH₃O(a)$_{Ti4c}$ species, the minor CH₃OH(a)$_{Ti5c}$ species barely accepts the photoexcited holes, subsequently exhibits no RHT process and is photo-inactive. Therefore, the adsorbed CH₃OH species on TiO₂ surfaces exhibit the site-sensitive electronic structures and subsequently the interfacial hole transfer processes (Scheme 1B). These results also suggest that the CH₃O(a)$_{Ti5c}$ species on anatase TiO₂(100)-(1×2) and TiO₂(101) surfaces are photoactive and responsible for the observed photocatalytic oxidation of CH₃O(a) species respectively on anatase TiO₂-{101} and TiO₂-{100}, whereas the minor CH₃O(a) species at the defective sites of anatase TiO₂(101) and TiO₂(100)-(1×2) surfaces are not. Similar theoretical calculation results were previously reported for the CH₃OH/rutile TiO₂(110) system.[17] This is different from the case in heterogeneous catalysis where minor defective sites usually contribute much to catalytic activity. Consequently, the experimental observations of photoactive CH₃O(a)$_{Ti5c}$ species on TiO₂-{101} and TiO₂-{100} NCs demonstrate the occurrence of CH₃OH dissociation at the surface Ti5c sites of anatase TiO₂(100)-(1×2) and TiO₂(101) surfaces.

Although the CH₃O(a)$_{Ti4c}$ species on the anatase TiO₂(001)-(1×4) surface and the CH₃O(a)$_{Ti5c}$ species on the anatase TiO₂(100)-(1×2) and TiO₂(101) surfaces exhibit the PDOS localized similarly at the VBM of corresponding TiO₂ surfaces, CH₃O(a)$_{Ti4c}$/TiO₂-{001} exhibits the largest photocatalytic oxidation rate constant (Fig. 4). All types of anatase TiO₂ NCs exhibit similar charge generation and separation efficiencies upon UV light illumination, thus this can be attributed, on one hand, to the most extensive upward surface band bending and subsequent the largest hole concentration on the TiO₂ surface for CH₃OH/TiO₂-{001}, on the other hand, to the fact that the minor CH₃OH(a) species barely competes with the dominant CH₃O(a)$_{Ti4c}$ species for the holes on TiO₂-{001}. Therefore, the site-sensitive adsorbed CH₃OH species on TiO₂ surfaces strongly affect the hole concentration on the surface and the photocatalytic efficiency by influencing the surface band bending and bulk-to-surface hole migration processes of TiO₂. With photoexcited charges-participated surface reactions as the rate-limiting step in photocatalytic reactions, a quasi equilibrium will establish for the photoexcited charges in the bulk and on the surface of photocatalysts, and the dynamics and concentration of photoexcited charges at the adsorbates/photocatalyst interfaces,

instead of their dynamics and concentration in the bulk, contributes to the photocatalytic reaction rate.

Photocatalytic activity of various TiO₂ NCs were evaluated in in gas-phase photocatalytic CH₃OH oxidation in O₂ to CO₂ under UV light illumination (Supplementary Fig. 26). The morphology-dependent photocatalytic activity were observed, in which TiO₂-{001} exhibits the highest CO₂ production while TiO₂-{100} is least. As shown above, the specific surface areas, the amounts of adsorbed O₂ and the bulk photoexcited charge carrier density are similar for various TiO₂ NCs, thus they are not responsible for the observed different photocatalytic behaviors. The observed morphology-dependent photocatalytic activity of various TiO₂ NCs can be reasonably related to the photocatalytic oxidation rate constants and surface coverages of photoactive CH₃OH adsorbates on various TiO₂ NCs. The photoactive CH₃O(a)$_{Ti4c}$ species on TiO₂-{001} NCs exhibits a higher photocatalytic oxidation rate constant and a larger surface coverage than the photoactive CH₃O(a)$_{Ti5c}$ species on TiO₂-{101} and TiO₂-{100} NCs, therefore, TiO₂-{001} NCs are more photocatalytic active than TiO₂-{101} and TiO₂-{100} NCs. These results demonstrate the key roles of site-dependent surface species and interfacial charge transfer in photocatalysis.
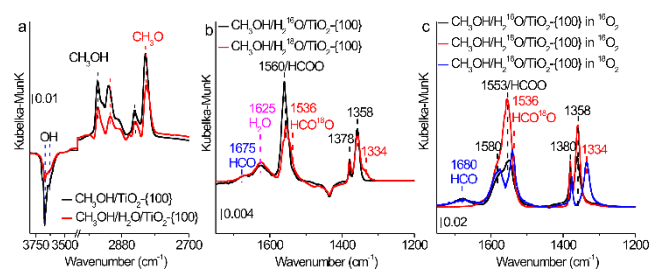

Figure 8. (a) DRIFTS spectra following CH₃OH adsorption on bare and water-precovered TiO₂-{100} NCs at 313 K, with DRIFTS spectra of corresponding bare TiO₂ NCs as the background spectra. (b) DRIFTS spectra after CH₃OH adsorption on H₂¹⁶O (H₂¹⁸O)-precovered TiO₂-{100} NCs at 313 K followed by UV light illumination, with corresponding DRIFTS spectra prior to UV light illumination as the background spectra. (c) DRIFTS spectra after CH₃OH adsorption on H₂¹⁶O (H₂¹⁸O)-precovered TiO₂-{100} NCs at 313 K followed by UV light illumination under a 10% ¹⁶O₂ (¹⁸O₂)/Ar atmosphere with a flow rate of 30 cm³/min, with corresponding DRIFTS spectra prior to UV light illumination as the background spectra.

Water was reported to affect the methanol photocatalysis over TiO₂ photocatalysts in various aspects,[4,14,38] such as influencing adsorption of reactants,[4,39] forming OH• radicals and/or additional surface-trapped holes,[40] and decelerating recombinative decay of holes.[41] Influences of water on photochemistry of CH₃OH on various TiO₂ NCs were examined. Exposure of water at 313 K on TiO₂ NCs forms molecularly-adsorbed H₂O(a) and various types of surface OH groups, whose intensities reduce greatly upon subsequent CH₃OH exposure, resulting from displacement of adsorbed H₂O(a) and OH groups by CH₃OH adsorption (Supplementary Fig. 28). The vibrational features of molecularly-adsorbed H₂O(a) disappears upon further evacuation. The DRIFTS spectra of CH₃OH adsorption on bare and H₂O-precovered TiO₂ NCs (Fig. 8a and Supplementary Fig. 28) show less formations of CH₃O(a) and CH₃OH(a) and less consumptions of original OH groups on H₂O-precovered TiO₂ NCs, indicating that pre-adsorption of water on TiO₂ NCs inhibits the subsequent adsorption of methanol by blocking the surface sites.

This leads to weaker intensities of photoexcited electrons in the in situ DRIFTS spectra of CH_3OH adsorption on H_2O-precovered TiO_2 NCs upon UV light illumination than on corresponding bare TiO_2 NCs, due to the decreased coverages of adsorbed methanol species that can efficiently trap photoexcited holes (Supplementary Fig. 29). In the presence of O_2, the intensity of photoexcited electrons in the in situ DRIFTS spectra of CH_3OH adsorption on H_2O-precovered TiO_2-{001} NCs upon UV light illumination is stronger than on bare TiO_2-{001} NCs. Thus, the pre-adsorption of water also inhibits the subsequent adsorption of O_2 that acts as efficient scavenger of photoexcited electrons. Meanwhile, the SPV measurements demonstrate less extensive upward surface band bending for CH_3OH adsorption on H_2O-precovered TiO_2 NCs than on corresponding bare TiO_2 NCs (Supplementary Fig. 30), resulting from the samller $CH_3O(a):CH_3OH$ ratios for CH_3OH adsorption on H_2O-precovered TiO_2 NCs. All these results demonstrate the adverse effects of pre-adsorbed water on the surface photochemistry of methanol on TiO_2 NCs.

Despite the above-observed adverse effects, we observed the photooxidation of methanol species on water-precovered TiO_2 NCs in the absence of O_2, evidenced by the appearances of the vibrational features of HCOO, HCO, OH and H_2O species at the expense of those of adsorbed methanol species in the DRIFTS spectra (Fig. 8b and Supplementary Fig. 31), although the coverages of formed surface intermediates are significantly lower than those formed during photooxidation of methanol species on bare TiO_2 NCs in the presence of O_2 (Supplementary Fig. 12). This is different from the case of methanol species on bare TiO_2 NCs in the absence of O_2, in which methanol species barely exhibits photooxidation reactivity (Supplementary Fig. 9). Thus, surface OH groups formed by water dissociation on TiO_2 NCs can act as the acceptor sites on TiO_2 surface for the injection of new electrons to trigger the photooxidation of adsorbed methanol species, forming the HCO and HCOO species. Moreover, the $HCO^{18}O$ species was observed In the DRIFTS spectra of methanol species on $H_2^{18}O$-precovered TiO_2-{100} NCs illuminated by UV light in the absence of O_2 (Fig. 8b and Supplementary Fig. 32), proving that the OH• radicals can directly oxidize the HCO intermediate. However, the major formate species is still $HCO^{16}O$, likely formed by oxidation of HCO intermediate by origially-existing ^{16}OH• radicals and by binding of HCO intermediate with surface lattice oxygen of TiO_2 ($HCO_{CH3OH}O_{TiO2}$). These observations demonstrate the existence of surface OH groups-induced photooxidation pathway of adsorbed methanol species on TiO_2 surface.

The abilities of surface OH group and O_2 to participate in photooxidation of adsorbed metahnol species on TiO_2 NCs were further examined by comparing surface photochemistry of adsorbed CH_3OH species on $H_2^{16}O$ ($H_2^{18}O$)-precovered TiO_2-{100} NCs at 313 K followed by UV light illumination in $^{16}O_2$ ($^{18}O_2$) (Fig. 8c and Supplementary Fig. 33). The HCO species, which emerges as the surface intermediate for photooxidation of $CH_3OH/H_2O/TiO_2$ in the absence of O_2 but not for for photooxidation of CH_3OH/TiO_2 in the presence of O_2, was observed for photooxidation of $CH_3OH/H_2^{16}O/TiO_2$ in the presence of O_2, implying the involvement of surface OH groups in photooxidation of adsorbed methanol species even in the presence of O_2. However, this species disappears for photooxidation of $CH_3OH/H_2^{18}O/TiO_2$ in the presence of O_2, which can be related to the isotope effect, including decreased coverage of OH groups on TiO_2 by $H_2^{18}O$ dissociation, comparing by $H_2^{16}O$ dissociation (Supplementary Fig. 34). No $HCO^{18}O$ species could be observed for photooxidation of $CH_3OH/H_2^{18}O/TiO_2$ in the presence of $^{16}O_2$. Moreover, for photooxidation of $CH_3OH/H_2^{16}O/TiO_2$ in the presence of $^{18}O_2$, only the COO stretch vibration features of $HCO^{18}O$ were observed, but those of the corresponding $HCO^{16}O$ species were not. Therefore, in the presence of O_2, surface OH groups on TiO_2 can still act as scavenger of photoexcited electrons to facilitate photooxidation of adsorbed methanol species, but the resulting OH• radicals seldom contribute to the formation of surface formate intermediates due to the presence of much more reactive O_2• radicals. It was also proposed that surface OH groups can open up a pathway of protonation in O_2 reduction to form •OOH radicals,[42] a species more reactive than the O_2• species in promoting the HCOO formation.[43] Similar to photooxidation of CH_3OH/TiO_2 in the presence of O_2 (Supplementary Fig. 12), an obvious vibration feature of carbonate at 1580 cm^{-1} was observed in all cases of photooxidation of $CH_3OH/H_2O/TiO_2$ in the presence of O_2 and does not exhibit the isotope effect. We tentatively assign this carbonate species to $CO_{CH3OH}O_{TiO2}O_{TiO2}$ strongly bound to TiO_2 surface.

Conclusion

In summary, we have successfully unveiled the site sensitive interfacial charge transfer and photocatalytic efficiency of CH_3OH oxidation on anatase TiO_2 NCs. The $CH_3O(a)_{Ti4c}$ species on TiO_2-{001} and the $CH_3O(a)_{Ti5c}$ species on TiO_2-{100} and TiO_2-{101} with the PDOS localized almost at the valence band maximum of corresponding TiO_2 surfaces are intrinsically more photoactive than the $CH_3OH(a)_{Ti5c}$ species with the PDOS localized within the valence band, while the $CH_3O(a)$ species at the defect-related sites is hardly photoactive. The $CH_3O(a)_{Ti4c}$ species of CH_3OH/TiO_2-{001} with the highest $CH_3O(a)$ coverage, the most extensive upward surface band bending and the largest hole concentration on the TiO_2 surface exhibits the largest photocatalytic oxidation rate constant. These results exemplify surface site- and adsorbate-dependent surface band bending/bulk-to-surface charge migration processes and electronic structure/interfacial charge transfer processes during photocatalytic reactions and demonstrate surface structure engineering of photocatalysts as an effective approach to maximize photocatalytic efficiencies.

Acknowledgements

Conflict of Interest

The authors declare no conflict of interest.

[1]   A. Fujishima, K. Honda, *Nature* **1972**, *238*, 37-38.
[2]   a) Y. Wang, et al, *Nat. Energy* **2019**, *4*, 746-760; b) U. Ulmer, T. Dingle, P. N. Duchesne, R. H. Morris, A. Tavasoli, T. Wood, G. A. Ozin, *Nat. Commun.* **2019**, *10*, 3169.
[3]   a) X. Chen, L. Liu, P. Y. Yu, S. S. Mao, *Science* **2011**, *331*, 746-750; b) R. Chen, S. Pang, H. An, J. Zhu, S. Ye, Y. Gao, F. Fan, C. Li, *Nat. Energy* **2018**, *3*, 655-663; c) B.-H. Lee, et al, *Nat. Mater.* **2019**, *18*, 620-626.
[4]   H. Chen, C. E. Nanayakkara, V. H. Grassian, *Chem. Rev* **2012**, *112*, 5919-5948.
[5]   a) S. Chen, F. Xiong, W. Huang, *Surf. Sci. Rep.* **2019**, *74*, 100471; b) L. Wu, C. Fu, W. Huang, *Phys. Chem. Chem. Phys.* **2020**, *22*, 9875-9909.
[6]   a) Z. Zhang, O. Bondarchuk, J. M. White, B. D. Kay, Z. Dohnálek, *J. Am. Chem. Soc.* **2006**, *128*, 4198-4199; b) Milena O'smic, Lars Mohrhusen, Katharina Al-Shamery, *J. Phys. Chem. C* **2019**, *123*, 7615-7626; c) F. Xiong, Y. Y.Yu, Z. Wu, G. Sun, L. Ding, Y. Jin, X. Q. Gong, W. Huang, *Angew. Chem. Int. Ed.* **2016**, *55*, 623-628.
[7]   M. Shen, M. A. Henderson, *J. Phys. Chem. Lett.* **2011**, *2*, 2707-2710.
[8]   C. Zhou, *et al.*, *Chem. Sci.* **2010**, *1*, 575-580.
[9]   a) Q. Guo, C. Xu, Z. Ren, W. Yang, Z. Ma, D. Dai, H. Fan, T. K. Minton, X. Yang, *J. Am. Chem. Soc.* **2012**, *134*, 13366-13373; b) M. Setvin, X. Shi, J. Hulva, T. Simschitz, G. S. Parkinson, M. Schmid, Valentin C. Di, A. Selloni, U. Diebold, *ACS Catal.* **2017**, *7*, 7081-7091.
[10]   a) K. R. Phillips, S. C. Jensen, M. Baron, S.-C. Li, C. M. Friend, *J. Am. Chem. Soc.* **2013**, *135*, 574-577; b) Q. Guo, C. Xu, W. Yang, Z. Ren, Z. Ma, D. Dai, T. K. Minton, X. Yang, *J. Phys. Chem. C* **2013**, *117*, 5293-5300; c) Q. Yuan, Z. Wu, Y. Jin, L. Xu, F. Xiong, Y. Ma, W. Huang, *J. Am. Chem. Soc.* **2013**, *135*, 5212-5219; d) X. Mao, Z. Wang, X. Lang, Q. Hao, B. Wen, D. Dai, C. Zhou, L.-M. Liu, X. Yang, *J. Phys. Chem. C* **2015**, *119*, 6121−6127; e) Z. Wang, Q. Yuan, Z. Zhang, F. Xiong, G. Sun, H. Xu, P. Chai, W. Huang, *J. Phys. Chem. C* **2019**, *123*, 31073-31081.
[11]   F. Xiong, L.-L. Yin, Z. Wang, Y. Jin, G. Sun, X.-Q. Gong, W. Huang, *J. Phys. Chem. C* **2017**, *121*, 9991-9999.
[12]   a) D. A. Bennett, M. Cargnello, T. R. Gordon, C. B. Murray, J. M. Vohs, *Phys. Chem. Chem. Phys.* **2015**, *17*, 17190-17201; b) D. A. Bennett, M. Cargnello, B. T. Diroll, C. B. Murray, J. M. Vohs, *Sur. Sci.* **2016**, *654*, 1-7.
[13]   D. A. Panayotov, S. P. Burrows, J. R. Morris, *J. Phys. Chem. C* **2012**, *116*, 6623-6635.
[14]   a) M. El-Roz, M. Kus, P. Cool, F. Thibault-Starzyk, *J. Phys. Chem. C* **2012**, *116*, 13252-13263.; b) M. El-Roz, P. Bazin, M. Daturi, F. Thibault-Starzyk, *ACS Catal.* **2013**, *3*, 2790-2798; c) M. El-Roz, P. Bazin, M. Daturi, F. Thibault-Starzyk, *Phys. Chem. Chem. Phys.* **2015**, *17*, 11277-11283.
[15]   Y. Tamaki, A. Furube, M. Murai, K. Hara, R. Katoh, M. Tachiya, *J. Am. Chem. Soc.* **2006**, *128*, 416-417.
[16]   X. Wang, A. Kafizas, X. Li, S. J. A. Moniz, P. J. T. Reardon, J. Tang, I. P. Parkin, J. R. Durrant, *J. Phys. Chem. C* **2015**, *119*, 10439-10447.
[17]   W. Chu, W. A. Saidi, Q. Zheng, Y. Xie, Z. Lan, O. V. Prezhdo, H. Petek, J. Zhao, *J. Am. Chem. Soc.* **2016**, *138*, 13740-13749.
[18]   D. Li, et al, *J. Phys. Chem. C* **2019**, *123*, 10367-10376.
[19]   D. Yang, D. Li, X. Liu, Y. Cao, Y. Gao, Y. R. Shen, W. T. Liu, *Proc. Natl. Acad. Sci.* **2018**, *115*, E3888-E3894..
[20]   a) T. Chen, Z. Feng, G. Wu, J. Shi, G. Ma, P. Ying, C. Li, *J. Phys. Chem. C* **2007**, *111*, 8005-8014; b) Z. Wang, F. Xiong, G. Sun, Y. Jin, W. Huang, *Chin. J. Chem.* **2017**, *35*, 889-895.
[21]   G. S. Foo, G. Hu, Z. D. Hood, M. Li, D.-e. Jiang, Z. Wu, *ACS Catal.* **2017**, *7*, 5345-5356.
[22]   Y. Li, *et al.*, *Nat. Commun.* **2017**, *8*, 581.
[23]   W. Yuan, Y. Wang, H. Li, H. Wu, Z. Zhang, A. Selloni, C. Sun, *Nano Lett.* **2016**, *16*, 132-137.
[24]   a) W. Hebenstreit, N. Ruzycki, G. S. Herman, Y. Gao, U. Diebold, *Phys. Rev. B* **2000**, *62*, R16334; b) A. Dahal, N. G. Petrik, Y. Wu, G. A. Kimmel,

[25]   a) N. Ruzycki, G. S. Herman, L. A. Boatner, U. Diebold, *Surf. Sci.* **2003**, *529*, L239-L244; b) M. Zuleta, S. Yu, S. Ahmadi, G. Boschloo, M. Göthelid, A. J. L. Hagfeldt, *Langmuir* **2010**, *26*, 13236-13244.
[26]   a) T. Berger, M. Sterrer, O. Diwald, E. Knözinger, D. Panayotov, T. L. Thompson, J. T. Yates, *J. Phys. Chem. B* **2005**, *109*, 6061-6068.; b) D. A. Panayotov, S. P. Burrows, J. R. Morris, *J. Phys. Chem. C* **2012**, *116*, 4535-4544.
[27]   a) R.-R. Feng, A.-A.Liu, S. Liu, J. Shi, R. Zhang, Z. Ren, *J. Phys. Chem. C* **2015**, *119*, 9798-9804; b) A. S. Crampton, L. Cai, N. Janvelyan, X. Zheng, C. M. Friend, *J. Phys. Chem. C* **2017**, *121*, 9910-9919.
[28]   a) A. Mattsson, S. L. Hu, K. Hermansson, L. Osterlund, *J. Vac. Sci. Technol. A*, **2014**, *32*, 061402; b) S. Chen, T. Cao, Y. Gao, D. Li, F. Xiong, W. Huang, *J. Phys. Chem. C* **2016**, *120*, 21472-21485; c) Y. Wang, B. Wen, A. Dahal, G. A. Kimmel, R. Rousseau, A. Selloni, N. G. Petrik, Z. Dohnálek, *J. Phys. Chem. C* **2020**, *124*, 20228−20239; d) X. Peng, R. Zhang, R.-R. Feng, A.-A. Liu, C. Zhou, Q. Guo, X. Yang, Y. Jiang, Z. Ren, *J. Phys. Chem. C* **2019**, *123*, 13789-13794;e) L. Ding, M. Li, Y. Zhao, H. Zhang, J. Shang, J. Zhong, H. Sheng, C. Chen, J. Zhao, *Appl. Catal. B-Environ.* **2020**, *266*, 118634; f) X. Chen, G. He, Y. Li, M. Chen, X. Qin, C. Zhang, H. He, *ACS Catal.* **2020**, *10*, 9706-9715; g) L.-F. Liao, W.-C. Wu, C.-Y. Chen, J.-L. Lin, *J. Phys. Chem. B* **2001**, *105*, 7678-7685.
[29]   D. Sporleder, D. P. Wilson, M. G. White, *J. Phys. Chem. C* **2009**, *113*, 13180-13191.
[30]   a) P. V. Kamat, I. Bedja, S. Hotchandani, *J. Phys. Chem.* **1994**, *98*, 9137-9142; b) D. W. Bahnemann, M. Hilgendorff, R. Memming, *J. Phys. Chem. B* **1997**, *101*, 4265-4275; c) T. Yoshihara, R. Katoh, A. Furube, Y. Tamaki, M. Murai, K. Hara, S. Murata, H. Arakawa, M. Tachiya, *J. Phys. Chem. B* **2004**, *108*, 3817-3823.
[31]   D. A. Wheeler, J. Z. Zhang, *Adv. Mater.* **2013**, *25*, 2878-2896.
[32]   a) S. Chen, D. Li, Y. Liu, W. Huang, *J. Catal.* **2016**, *341*, 126-135; b) F. J. Knorr, C. C. Mercado, J. L. McHale, *J. Phys. Chem. C* **2008**, *112*, 12786-12794. c) C. C. Mercado, F. J. Knorr, J. L. McHale, S. M. Usmani, A. S. Ichimura, L. V. Saraf, *J. Phys. Chem. C* **2012**, *116*, 10796-10804.
[33]   M. D'Arienzo, J. Carbajo, A. Bahamonde, M. Crippa, S. Polizzi, R. Scotti, L. Wahba, F. Morazzoni, *J. Am. Chem. Soc.* **2011**, *133*, 17652-17661.
[34]   a) P. Maity, O. F. Mohammed, K. Katsiev, H. Idriss, *J. Phys. Chem. C* **2018**, *122*, 8925-8932; b) M. Xu, Y. Gao, E. Martinez Moreno, M. Kunst, M. Muhler, Y. Wang, H. Idriss, C. Wöll, *Phys. Rev. Lett.* **2011**, *106*, 138302; c) M. A. Nadeem, G. I. A. Waterhouse, H. Idress, *Surf. Sci.* **2016**, *650*, 40-50.
[35]   C. Guo, X. Meng, H. Fu, Q. Wang, H. Wang, Y. Tian, J. Peng, R. Ma, Y. Weng, S. Meng, E. Wang, Y. Jiang, *Phys. Rev.Lett.* **2020**, *124*, 206801.
[36]   Z. Zhang, J.T. Yates, *Chem. Rev.* **2012**, *112*, 5520−5551.
[37]   Z. Chen, Q. Zhang, Y. Luo, *Angew. Chem. Int. Ed.* **2018**, *57*, 5320-5324.
[38]   G. L. Chiarello, D. Ferri, E. Selli, *J. Catal.* **2011**, *280*, 168-177.
[39]   a) M. Shen, M. A. Henderson, *J. Phys. Chem. C* **2012**, *116*, 18788-18795; b) C. Xu, W. Yang, Q. Guo, D. Dai, M. Chen, X. Yang, *Chin. J. Catal.* **2014**, *35*, 416-422.
[40]   a) A. Y. Ahmed, T. A. Kandiel, T. Oekermann, D. Bahnemann, *J. Phys. Chem. Lett.* **2011**, *2*, 2461-2465; b) A. Y. Ahmed, T. A. Kandiel, I. Ivanova, D. J. A. S. S. Bahnemann, *Appl. Surf. Sci.* **2014**, *319*, 44-49; c) G. L. Chiarello, D. Ferri, E. Selli, *J. Catal.* **2011**, *280*, 168-177.
[41]   A. Yamakata, T.-a. Ishibashi, H. Onishi, *J. Phys. Chem. B* **2003**, *107*, 9820-9823.
[42]   a) Y. Du, N. A. Deskins, Z. Zhang, Z. Dohnálek, M. Dupuis, I. Lyubinetsky, *J. Phys. Chem. C* **2009**, *113*, 666-671; b) H. Song, X. Meng, S. Wang, W. Zhou, X. Wang, T. Kako, J. Ye, *J. Am. Chem. Soc.* **2019**, *141*, 20507-20515.
[43]   Y. Nosaka, A. Y. Nosaka, *Chem. Rev.* **2017**, *117*, 11302-11336.

Layout 1:

Research Article

Surface sites and resulting methanol adsorbates strongly affect the surface band bending/bulk-to-surface charge migration processes and the interfacial electronic structure/interfacial charge transfer processes, and consequently play a key role in the photocatalytic efficiency.
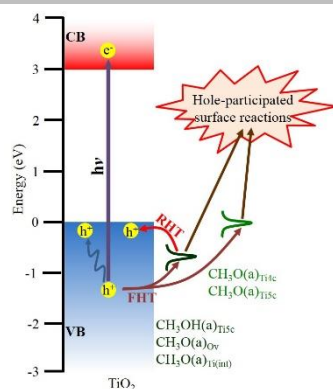
Cong Fu,[+] Fei Li,[+] Jiachen Zhang,[+] Dan Li, Kun Qian, Yong Liu, Junwang Tang, Fengtao Fan, Qun Zhang,[*] Xue-Qing Gong,[*] Weixin Huang[*]

Page No. – Page No.

Site Sensitivity of Interfacial Charge Transfer and Photocatalytic Efficiency in Photocatalysis